INTERACTIONS OF NOCTURNAL SLOPE FLOWS WITH AMBIENT WINDS

RAYMOND W. ARRITT

Cooperative Institute for Research in the Atmosphere, Colorado State University, Ft. Collins, CO 80523, U.S.A.

and

ROGER A. PIELKE

Department of Atmospheric Science, Colorado State University, Ft. Collins, CO 80523, U.S.A.

(Received in final form 9 June, 1986)

Abstract. A quasi-one-dimensional numerical model containing a prognostic turbulent kinetic energy parameterization and simplified approximations to horizontal gradients is used to study interactions of thermally induced nocturnal slope flows with following and opposing ambient winds. It is found that a following ambient wind causes the peak perturbation wind to be weaker and to be realized at a greater height, while an opposing ambient wind leads to a stronger perturbation wind at a lower height. The reason for this response lies in the interactions of the shears of the thermal and ambient components through the mechanical production of turbulent kinetic energy.

Nomenclature

a constant in TKE closure scheme ($a = 0.2$),
E turbulent kinetic energy,
f Coriolis parameter,
g acceleration of gravity,
k von Karman constant,
K_h eddy exchange coefficient for scalars,
K_m eddy exchange coefficient for momentum,
l_h turbulent length scale for scalars,
l_m turbulent length scale for momentum,
n pseudo-vertical coordinate (perpendicular to ground),
Ri_f flux Richardson number,
s downslope distance; $s = 0$ at crest of slope,
t time,
u, velocity component, positive downslope,
u_g geostrophic part of u,
v cross-slope velocity,
v_g geostrophic part of v,
w velocity component in n direction,
β slope angle,
γ ambient potential temperature lapse rate,
θ potential temperature.

Boundary-Layer Meteorology **37** (1986) 183–195.

1. Introduction

Nocturnal thermally induced slope winds can substantially influence the dispersion of atmospheric pollutants, as demonstrated in the U.S. Department of Energy Atmospheric Studies in Complex Terrain (ASCOT) program (Dickerson and Gudiksen, 1983). Slope winds can also be important in the generation of larger scale flows, such as valley-axis winds which can be produced when a valley fills with cold air to create a horizontal pressure gradient between the valley interior and the corresponding height over an adjacent plain (Defant, 1951; McNider and Pielke, 1984). An understanding of nocturnal slope winds is thus desirable in order to describe the evolution of nocturnal boundary layers over complex terrain.

The interactions of thermally forced slope flows with prevailing ambient winds are incompletely understood, as noted for example by Egan (1984). Effords in this direction include those of Lykosov and Gutman (1972), who extended Prandtl's (1942) analytic model to include ambient winds, and Fitzjarrald (1984), who used a layer-average model to study phenomena such as the delay of onset of katabatic winds due to an opposing ambient flow. While these analytic methods provide useful insight, they involve simplifying assumptions which can be rather restrictive. The solution of Lykosov and Gutman, for example, uses an eddy viscosity which is constant with height rather than varying with stability and height above the surface as would be more realistic. The layer-average approach used by Fitzjarrald and others by its nature cannot provide details of the vertical structure of the flow.

Multidimensional numerical models have been used by investigators such as Mannouji (1982), Yamada (1983), and McNider and Pielke (1984) to study nocturnal slope flows. Such models provide very complete descriptions of the flows, but this must be weighed against the models' complexity and expense, and the need to discretize the governing equations. As an intermediate step, we have adopted a numerical model in which only the dimension perpendicular to the ground is explicitly considered. The model is not truly one-dimensional because simplified representations of horizontal gradients are employed.

We shall use the quasi-one-dimensional numerical model to investigate interactions of nocturnal slope flows with ambient winds. The numerical model incorporates both ambient winds and a more realistic treatment of turbulence than is possible in an analytic solution. The use of a prognostic turbulent kinetic energy equation also permits analysis of the turbulence budgets of the predicted slope flows, so that the fundamental processes which are active in the generation of the slope flow profiles can be assessed.

2. Model Formulation and Verification

The quasi-one-dimensional model is similar to the formulations used by Rao and Snodgrass (1981) and Doran and Horst (1983). A slope-aligned (s, y, n) coordinate is used which is analogous to a cartesian (x, y, z) system tilted by the slope angle (Figure 1). The slope is assumed to be two-dimensional, so that all gradients in the

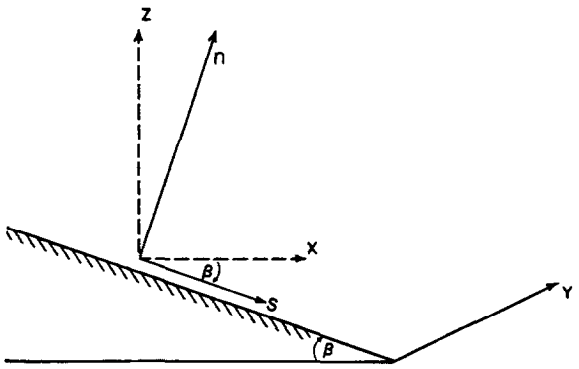

Fig. 1. Slope-aligned (s, y, n) coordinate (solid lines) compared to Cartesian (x, y, z) coordinate (dashed).

y-dimension are zero. Prognostic equations are solved for u momentum, v momentum, and potential temperature:

$$\frac{\partial u}{\partial t} = -g\,\frac{\theta'}{\bar{\theta}}\,\sin\beta + f(v - v_g) - u\,\frac{\partial u}{\partial s} - w\,\frac{\partial u}{\partial n} + \frac{\partial}{\partial n}\left(K_m\,\frac{\partial u}{\partial n}\right), \tag{1}$$

$$\frac{\partial v}{\partial t} = -f(u - u_g) - u\,\frac{\partial v}{\partial s} - w\,\frac{\partial v}{\partial n} + \frac{\partial}{\partial n}\left(K_m\,\frac{\partial v}{\partial n}\right), \tag{2}$$

$$\frac{\partial \theta'}{\partial t} = -\left[u'\gamma\sin\beta + u\,\frac{\partial \theta'}{\partial s}\right] - w\,\frac{\partial \theta'}{\partial n} + \frac{\partial}{\partial n}\left(K_h\,\frac{\partial \theta'}{\partial n}\right). \tag{3}$$

In addition, there is a diagnostic relationship for vertical velocity derived from the incompressible continuity equation:

$$\frac{\partial w}{\partial n} = -\frac{\partial u}{\partial s}\,. \tag{4}$$

In Equations (1)–(3), overbars represent values of the ambient profiles and primed quantities represent perturbations from the ambient state, e.g., $\theta'(z) = \theta(z) - \bar{\theta}(z)$, where $\bar{\theta}(z)$ is the unperturbed ambient value. The form of the horizontal advection of potential temperature (bracketed term in Equation (3)) assumes that the ambient potential temperature field is in equilibrium with the ambient wind field. Therefore, the total wind advects only the perturbation potential temperature, while the ambient potential temperature structure is advected only by the perturbation wind. Following Doran and Horst (1983), advection of perturbation quantities is neglected when the total wind is upslope, because downslope (upstream for $u < 0$) information on the perturbation gradients is unavailable. The advection and divergence terms are otherwise approximated by assuming linear gradients between the crest of the slope ($s = 0$) and the

location of interest. In calculating these gradients, it is also assumed that the profile at $s = 0$ is unaffected by the slope flow.

The initial potential temperature profile is constructed using an initial surface value of potential temperature and a constant lapse rate, γ. The initial wind profile is found by integrating (1) and (2) for one inertial cycle assuming a constant geostrophic wind speed. During this initial integration, the exchange coefficients are found using the profile method of O'Brien (1970). We equate the 'initial' and 'ambient' temperature and wind profiles; the ambient profiles remain constant through the course of the simulation.

The exchange coefficients, K_m and K_h, are derived using the method employed by Rao and Snodgrass (1981), which is adapted from Delage (1974). This parameterization is based on a prognostic turbulent kinetic energy (TKE) equation,

$$\frac{\partial E}{\partial t} = K_m \left[\left(\frac{\partial u}{\partial n} \right)^2 + \left(\frac{\partial v}{\partial n} \right)^2 \right] - K_h \frac{g}{\theta} \frac{\partial \theta}{\partial n} + \frac{\partial}{\partial n} \left(K_m \frac{\partial E}{\partial n} \right) + (1 - Ri_f) \frac{a^2 E^2}{K_m} \tag{5}$$

and diagnostic length scales,

$$l_m = \frac{kz}{\phi_m} , \tag{6a}$$

$$l_h = \frac{kz}{\phi_h} . \tag{6b}$$

The exchange coefficients are then represented as

$$K_m = l_m (aE)^{1/2} , \tag{7a}$$

$$K_h = l_h (aE)^{1/2} . \tag{7b}$$

The variable k is von Karman's constant, and the constant a is set to 0.2. This is not an adjustable parameter, as the value $a = 0.2$ was specified before the first execution of the model and remained unchanged. Values of the non-dimensional profile functions ϕ_m and ϕ_h are calculated according to the formulas of Businger *et al.* (1971).

Numerical solution is by forward time differencing on all time tendencies. Linear-upstream spatial differencing is used for the vertical advection terms. It is recognized that linear-upstream differencing is rather inaccurate (Pielke, 1984); however, we feel that the simplistic representation of the horizontal divergence (and thus of vertical velocity) does not justify the much greater computational expense of more accurate schemes such as the cubic spline or finite element methods. Vertical diffusion is solved explicitly. The explicit method is highly accurate for small Fourier numbers (Pielke, 1984) and is computed very efficiently on a vector processor such as the Cray–1A system.

The model was verified using the 1–2 July, 1980 slope flow data from the ASCOT observations at Rattlesnake Mountain (Horst and Doran, 1982; Doran and Horst, 1983). The surface cooling rate for this case was approximated by an initial cooling of

4 K with further cooling of 0.5 K hr^{-1} for 4 hr as deduced from the aformentioned studies, so that the predicted profiles correspond approximately to midnight. Figure 2 compares the predicted velocity and potential temperature profiles (solid curves) to the observed values (darkened circles). The agreement of the predictions to the observations is generally good. The slope flow velocity maximum is underpredicted by about 0.2 m s^{-1}, with the overall shape of the predicted profile similar to that of the observations. The potential temperature is underpredicted by about 0.5 K at 1.2 and 2.1 m, with smaller errors at the higher elevations.

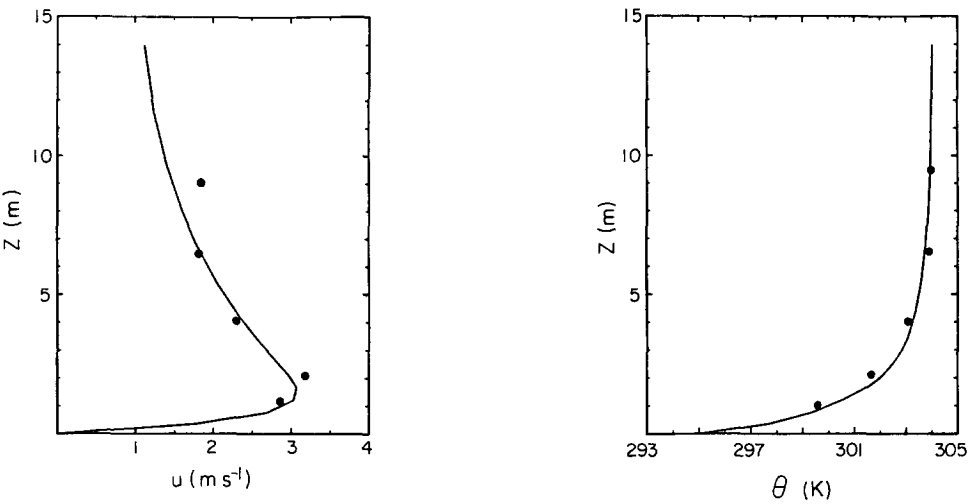

Fig. 2. Predicted (a) velocity and (b) potential temperature profiles for 1–2 July, 1980 Rattlesnake Mountain case (solid curves) compared to observed data (darkened circles).

The ability of the model to reproduce observed data with reasonable accuracy permits a more detailed analysis of the processes which are active in the evolution of the flow. We shall first examine a baseline case with no ambient winds, and then consider deviations from this baseline due to the presence of ambient winds.

3. Slope Flow Baseline Case

The initial and boundary conditions for the baseline case are specified in Table I. The ambient potential temperature stratification of $\gamma = 1$ K km^{-1} is typical of a slightly stabilized mixed layer shortly after sunset. We used the same cooling for this case (and the cases to follow) as in the Rattlesnake Mountain case. The lack of ambient flow in the baseline case allows a more systematic examination of the influence of ambient winds.

The predicted velocity, potential temperature, and turbulent kinetic energy profiles after four hours of cooling are presented in Figure 3. Of particular interest is the local

TABLE I

Model specifications for slope flow baseline case

Ambient winds	$u_g = v_g = 0$
Ambient potential temperature stratification	$\gamma = 1$ K km^{-1}
Slope angle	$\beta = 10°$
Downslope distance	$s = 1$ km
Roughness length	$z_0 = 0.01$ m
Surface cooling	initial $\theta_0' = -4$ K further cooling 0.5 K hr^{-1} for 4 hr
Coriolis parameter	$f = 10^{-4}$ s^{-1}
Vertical levels	0.35, 0.75, 1.2, 1.65, 2.1 2.65, 3.4, 4.3, 5.4, 6.8, 8, 9.7, 11.6, 14, 17, 20.5, 24.5, 30, 36.5, 44, 52, 62, 73, 87, 105, 125, 150, 180, 220, 270, ... (Δn = 60 m) ... 1470 m

minimum of TKE near the resolvable velocity maximum or 'jet'. The local value of the vertical shear of the slope flow velocity is zero at the jet maximum, so that the mechanical production of TKE (first term in Equation (5)) vanishes. The TKE is non-zero at the jet maximum due to the diffusion of TKE into the jet region from above and below (third term in Equation (5)). The magnitudes of the TKE forcing terms are shown in Figure 4.

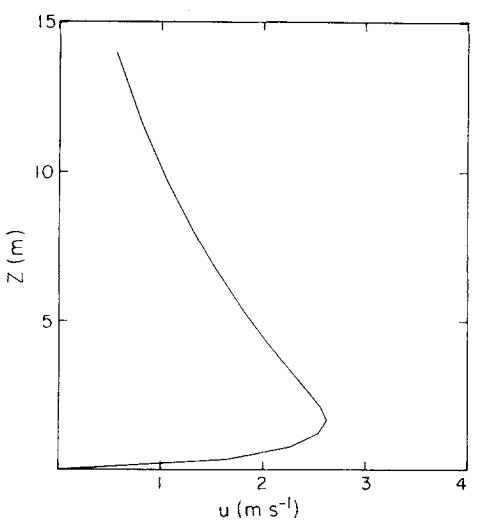

Fig. 3a.

Figs. 3a–c. Predicted (a) velocity, (b) potential temperature, and (c) turbulent kinetic energy profiles for slope flow baseline case.

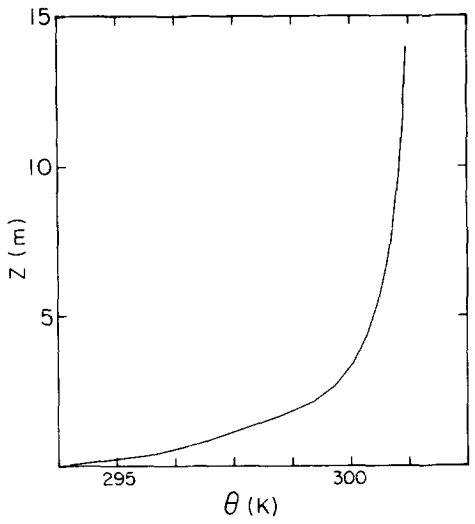

Fig. 3b.

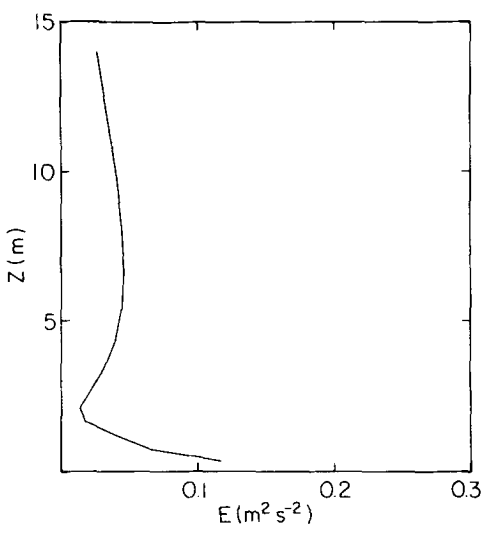

Fig. 3c.

The importance of the TKE diffusion term is illustrated by the unrealistic solutions which are obtained when the term is neglected (Figure 5). Comparison of these profiles to the baseline solutions (Figure 3) shows that there is inadequate mixing across the jet, indicating that a turbulence scheme which is to be applied to nocturnal slope flows must contain a method to allow turbulent transfer across the jet maximum. The TKE diffusion term in equation (5) and other prognostic TKE formulations (e.g., Yamada, 1983) perform this function. A TKE-based method which relies on a production-dissipation balance, such as the level 2 scheme of Mellor and Yamada (1982), must allow turbulent exchange across the jet maximum if nocturnal slope flows are to be properly simulated.

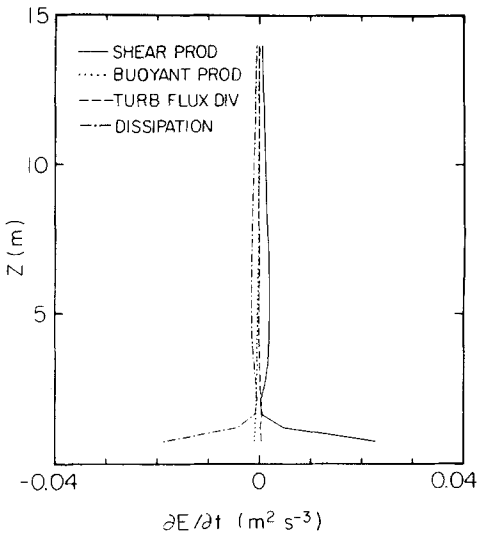

Fig. 4. Turbulent kinetic energy budget for slope flow baseline case. Solid curve, mechanical production; dotted curve, buoyant production; dashed curve, turbulent flux convergence; dash-dot dissipation.

4. Slope Flow Interactions with Ambient Winds

We now use the quasi-one-dimensional model to examine situations in which the slope flow is embedded in an ambient wind. Two cases are simulated: one with a downslope (or 'following') ambient wind, $u_g = 2$ m s^{-1}, and the other with an opposing ambient

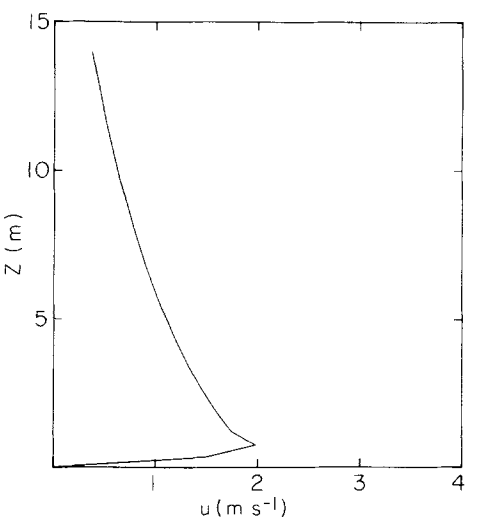

Fig. 5a.

Figs. 5a–c. As Figure 3, except omitting the turbulent diffusion of TKE.

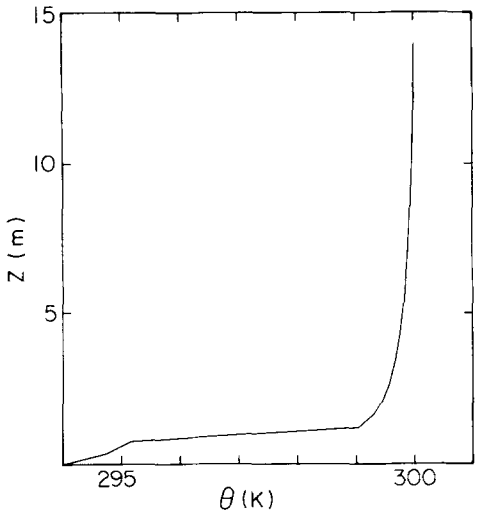

Fig. 5b.

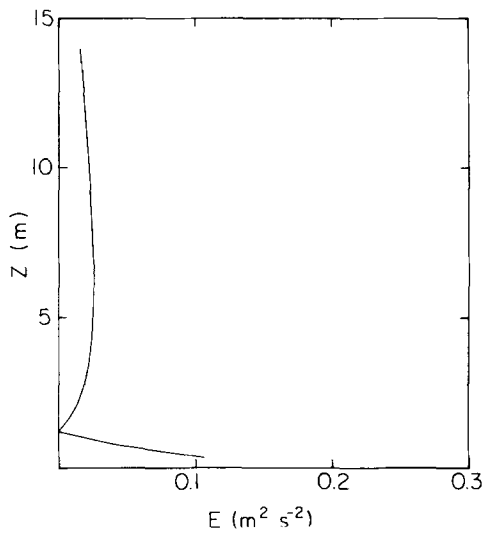

Fig. 5c.

wind, $u_g = -2$ m s^{-1}. All other model parameters are as specified in the baseline case. The model solutions are shown both as the total predicted wind and as the pertubations from the ambient wind. The former represents values which would be observed in the field, while the latter allows a more focused examination of the thermally induced component of the flow.

Figure 6 shows the total predicted velocity profiles, and Figure 7 gives the perturbation profiles. It is apparent that while the total velocity increases with a following ambient wind, the peak perturbation velocity decreases. The peak perturbation velocity

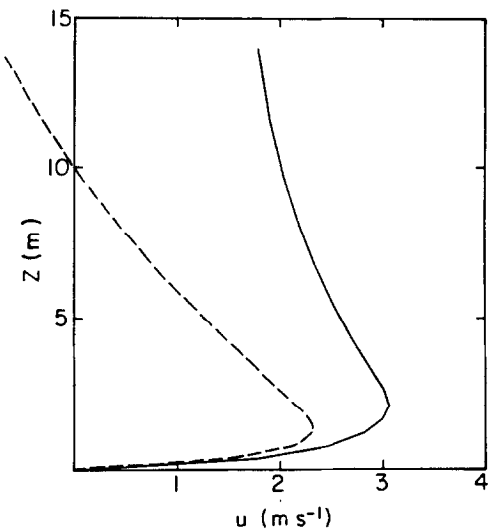

Fig. 6. Predicted total velocity profiles after four hours for cases with following ambient wind, $u_g = 2$ m s^{-1} (solid curve), and opposing ambient wind, $u_g = -2$ m s^{-1} (dashed curve).

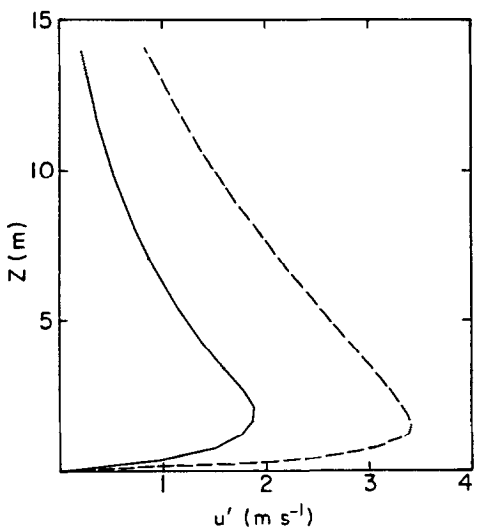

Fig. 7. As Figure 6, except perturbation velocity profiles.

is also obtained at a somewhat greater height with a following wind than with no ambient wind. The opposite response is predicted for the case of opposing ambient flow, i.e., the total velocity decreases but the perturbation velocity increases.

The explanation of the effect of ambient winds on the perturbation velocity profile lies in the relationship of the shear of the ambient wind to the shear of the thermally induced component. The latter always has positive shear below the jet (i.e., $du/dz > 0$) for the

slope configuration used here. A following ambient wind also has positive shear, so that the shear of the total wind is greater than if no ambient wind were present. This leads to an increase in the mechanical production of TKE and an increase in the turbulent transfer of momentum toward the ground. With an opposing ambient wind, the shear of the thermally-induced and ambient components are of opposite sign. Therefore, the total shear is less than with no ambient wind, so that there is less frictional retardation and the perturbation velocity increases. Figure 8 gives the turbulence budgets for each

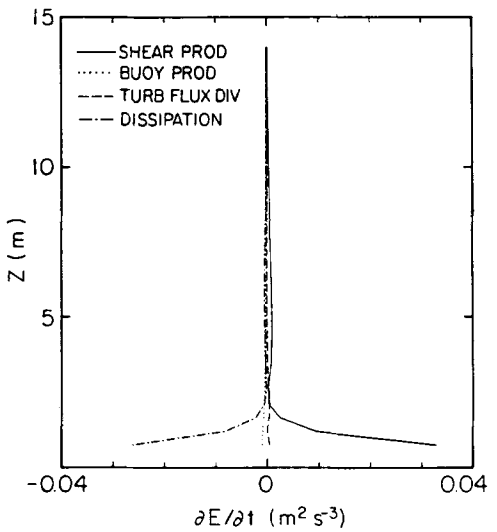

Fig. 8a.

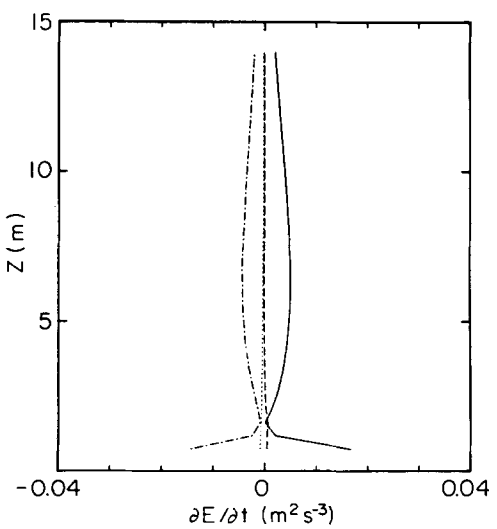

Fig. 8b.

Figs. 8a–b. Turbulent kinetic energy budgets for cases with (a) following ambient wind, $u_g = 2\ \mathrm{m\ s^{-1}}$; (b) opposing ambient wind, $u_g = -2\ \mathrm{m\ s^{-1}}$. Interpretation of curves as in Figure 4.

of the simulations with ambient winds, showing that the mechanical production of turbulent kinetic energy below the jet maximum increases with a following ambient wind and decreases with an opposing wind.

These results indicate that the development of nocturnal katabatic flow is altered by the presence of ambient winds, and that this interaction must be accounted for in order to obtain accurate representations of nocturnal winds over sloping terrain. A slope flow solution for zero ambient wind (such as that of Prandtl, 1942) cannot simply be linearly added to an ambient wind profile.

5. Conclusions

The baseline case turbulence budget indicates that the TKE diffusion term is important to the evolution of nocturnal slope flows, even though its absolute magnitude is rather small. This is because the diffusion of TKE permits turbulent transfer across the jet maximum, where the vertical shear of the downslope wind tends to zero and the local Richardson number becomes large. Solutions obtained when this term is neglected are quite unrealistic. Therefore, a turbulence scheme which is to be applied to nocturnal slope flows should provide a mechanism to permit turbulent transfer across the jet maximum.

The simulations with ambient winds show that ambient winds interact nonlinearly with the thermally induced component. Examination of the katabatic flows as perturbations from the ambient wind profiles indicates that a following ambient wind causes the perturbation to decrease and to be obtained at a greater height, while an opposing wind results in a stronger thermally induced perturbation obtained at a lower height. These nonlinear interactions indicate that the linear superposition of separate profiles for the ambient and thermally induced component will not yield an accurate profile of the total wind.

Acknowledgements

This research was sponsored by the U.S. National Park Service under contract NA81RAH0001, Amendment 17, Item 15, by the Electric Power Research Institute under contract RP-1630-53, and by the National Science Foundation under grant ATM-8414181. Computations were performed at the National Center for Atmospheric Research, which is sponsored by the National Science Foundation. We wish to thank J. C. Doran for furnishing the Rattlesnake Mountain data and R. T. McNider for discussions on nocturnal slope flows.

References

Defant, F.: 1951, 'Local Winds', *Compendium of Meteorology*, American Meteorological Society, pp. 655–672.

Delage, Y.: 1974, 'A Numerical Study of the Nocturnal Atmospheric Boundary Layer', *Quart. J. Roy. Meteorol. Soc.* **100**, 351–364.

Dickerson, M. H. and Gudiksen P. H.: 1983, *Atmospheric Studies in Complex Terrain: Technical Progress Report FY–1979 through FY–1983*, 367 pp.

Doran, J. C. and Horst, T. W.: 1983, 'Observations and Models of Simple Nocturnal Slope Flows', *J. Atmos. Sci.* **40**, 708–717.

Egan, B. A.: 1984, Transport and Diffusion in Complex Terrain (Review), *Boundary-Layer Meteorol.* **30**, 3–28.

Fitzjarrald, D. R.: 1984, 'Katabatic Wind in Opposing Flow', *J. Atmos. Sci.* **41**, 1143–1158.

Horst, T. W. and Doran, J. C.: 1982, *Simple Nocturnal Slope Flow Data from the Rattlesnake Mountain Site*, Pacific Northwest Laboratory, Richland, Washington U.S.A., 98 pp.

Lykosov, V. N. and Gutman L. N.: 1972, 'Turbulent Boundary Layer Above a Sloping Underlying Surface', *Izv. Atmos. Ocean. Phys.* **8**, 799–809.

Mannouji, N., 1982: 'A Numerical Experiment on the Mountain and Valley Winds', *J. Meteorol. Soc. Japan* **60**, 1085–1105.

McNider, R. T. and Pielke, R. A.: 1981, 'Diurnal Boundary-Layer Development Over Sloping Terrain', *J. Atmos. Sci.* **38**, 2198–2212.

McNider, R. T. and Pielke R. A.: 1984, 'Numerical Simulation of Slope and Mountain Flows', *J. Clim. Appl. Meteorol.* **23**, 1441–1453.

Mellor, G. L. and Yamada, T.: 1982, 'Development of a Turbulence Closure Model for Geophysical Fluid Problems', *J. Geophys. Res.* **20**, 851–875.

O'Brien, J. J.: 1970, 'A Note on the Vertical Structure of the Eddy Exchange Coefficient in the Planetary Boundary Layer', *J. Atmos. Sci.* **27**, 1213–1215.

Pielke, R. A.: 1984, *Mesoscale Meteorological Modeling*, Academic Press, 612 pp.

Prandtl, L.: 1942, *Fuhrer durch die Stromungslehre*, Verslag Vieweg und Sohn, Braunschweig, Germany.

Rao, K. S. and Snodgrass, H. F.: 1981, 'A Nonstationary Nocturnal Drainage Flow Model', *Boundary-Layer Meteorol.* **20**, 309–320.

Yamada, T.: 1983, 'Simulations of Nocturnal Drainage Flows by a q^2l turbulence Closure Model', *J. Atmos. Sci.* **40**, 91–106.